의학석사 학위논문

관상동맥 협착 병변의 형태 및 혈류역학적 지표가 동맥경화반의 취약성에 미치는 영향

Influence of Coronary Stenosis Geometry and Hemodynamic Parameters on Plaque Vulnerability

2017년 8월

서울대학교 대학원

의학과 내과학 전공

Jinlong Zhang

Abstract

Objectives: The objective of this study was to investigate the influence of lesion geometry and hemodynamic parameters on plaque vulnerability.

Background: The relationship among lesion geometry, hemodynamic forces acting on the plaque, location and presence of vulnerable features has not been explored.

Methods: Seventy-one patients (73 lesions) with fractional flow reserve (FFR) measurement in addition to at least one imaging device [intravascular ultrasound (IVUS) or optical coherence tomography (OCT)] were enrolled. Differences of FFR, trans-stenotic FFR gradient (△FFR) and trans-stenotic pressure gradient (△P) between lesions with and without vulnerable features were investigated. Radius gradient (RG), measured by standard method and, also, measured on point of 2.5mm, 5mm, 7.5mm away from MLA point, were respectively calculated using IVUS. Axial plaque stress (APS) were calculated using intracoronary pressure and RG.

Upstream-dominant lesions were defined as lesions with $RG_{upstream} > RG_{downstream}$. The longitudinal distribution of APS between two segments [upstream, downstream divided by minimum lumen area (MLA)] was compared according to lesion asymmetry. Presence of vulnerable features was compared among three segments (upstream, MLA, downstream) according to lesion asymmetry.

Results: FFR was significantly lower in lesions with lipid rich plaque than those without lipid rich plaque [0.79(0.73-0.82) vs. 0.82(0.80-0.93) p = 0.038]. Significantly bigger △P was shown in lesions with microvessel(s) [12.5(8.0-21.3) vs. 7.5(5.0-14.8) p= 0.045]. Significant bigger △FFR between lesions with posterior attenuation was shown compared to those without posterior attenuation [0.19(0.11-0.36) vs. 0.10(0.08-0.16) p = 0.038]. Among several different RG measurements, RG calculated from point of 5mm away from MLA showed not only the best reliability [intraclass correlation coefficient (ICC) = 0.924]] but the best correlation (r = 0.904 p < 0.001) with RG measured using standard method. The significantly higher APSs were observed in the

upstream segments of upstream-dominant lesions than those of downstream-dominant lesions (9.78 ± 4.81 vs. 6.30 ± 3.89 p = 0.003) and downstream segments of downstream-dominant lesions than those of upstream-dominant lesions (8.25 ± 3.38 vs. 4.36 ± 2.68 p < 0.001). The frequency of lipid rich plaque in addition to posterior attenuated plaque was lowest in the downstream segments compared to the upstream and MLA segments of downstream-dominant lesions (upstream vs. MLA vs. downstream 53.3% vs. 53.3% vs. 13.3% p = 0.011). The appearance of maximum lipid arc and posterior attenuation arc was rarely observed in downstream segments of downstream-dominant lesions (upstream vs. MLA vs. downstream 35.7% vs. 64.3% vs. 0% p = 0.013).

Conclusions: Hemodynamic parameters, FFR, △FFR and △P show differences between lesions with and without lipid rich plaque, microvessel(s) and posterior attenuation. While, APS seems not to play a crucial role in distribution of vulnerable features, its force directly impacting on plaque appears to contribute to plaque rupture only.

Key Words: Coronary plaque; Vulnerable plaque; Fractional flow reserve; Radius gradient; Axial plaque stress; Intravascular ultrasound; Optical coherence tomography.

Student Number: 2015-22406

List of Figures and Tables

List of Abbreviations

ACS = acute coronary syndrome

APS = axial plaque stress

QCA = quantitative coronary angiography

MLD = minimal lumen diameter

%DS = percent diameter stenosis

IVUS = intravascular ultrasound

MLA = minimal lumen area

%PB = percent plaque burden

OCT = optical coherence tomography

TCFA = thin cap fibroatheroma

FFR = fractional flow reserve

RG = radius gradient

APS = axial plaque stress

WSS = wall shear stress

Contents

Introduction

Coronary plaque rupture is a well-known pathophysiological trigger of acute coronary syndrome (ACS).[1-8] Although previous studies have shown the mechanism of plaque rupture, the prediction of plaque rupture is, even now, problematic. The plaque rupture can occur whenever the plaque strength can't sustain the increasing plaque stress.[9,10] Many studies have explored the imaging-based intrinsic properties of individual plaque which can increase the risk of plaque rupture.[1-8] However, the relationship between extrinsic forces acting on the plaque and plaque vulnerability has not been clearly defined.[11-13]

Among several components of hemodynamic forces acting on plaque, wall shear stress (WSS) has been known as a key force which plays a crucial role in plaque initiation, progression, and transformation into a vulnerable phenotype.[6,9,14,15] However, the magnitude of WSS is extremely minimal compared with other components of hemodynamic forces. Therefore, what is clear is

WSS alone cannot directly lead to plaque rupture. By contrast, a net anterograde axial force, which was determined by pressure gradient, would increase the axial tension and stress in the upstream segment of the lesion but decrease those in the downstream segment. The retrograde axial force on the plaque can also occur by certain plaque geometries despite the tiny pressure gradient in the downstream segment. Such a net axial force which named axial plaque stress (APS) fully gives a reasonable explanation of both upstream and downstream plaque rupture. The lesion geometry largely determines the distribution of APS, and, even more, is associated with not only the location of rupture but the clinical presentation.[11,12,16,17]

The objective of this study was to investigate the influence of lesion geometry and hemodynamic parameters on plaque vulnerability in patient with the invasive fractional flow reserve (FFR) measurement as well as at least one imaging device – either intravascular ultrasound (IVUS) or optical coherence tomography (OCT). In addition, we attempted to reproduce invasively the

relationship between hemodynamic force and lesion geometry which observed by recent study using computational fluid dynamics (CFD) models.

Methods

Patient Population

The study flow has been shown previously. (**Fig. 1**). Between October 2014 and January 2016, 108 consecutive patients with 114 intermediate stenosis were selected from 4 university hospitals in Korea. The inclusion criteria were patients (1) with coronary artery disease, which was caused by de novo lesions and had one or more visually estimated 40%-70% stenosis of vessel diameter; (2) with measurement of FFR and pressure wire pull back tracing, in addition to IVUS or OCT. We excluded lesions (1) from distal portion or any branch of major native coronary artery; (2) with poor image quality; (3) with unevaluable plaque geometry due to diffuse (> 40 mm) or focal (< 6 mm) structure. The study protocol was approved by the institutional review board or ethics committee at each participating center, and was in accordance with the Declaration of Helsinki.

Coronary Angiography and Quantitative Coronary Angiography

Analysis

Invasive coronary angiography was performed utilizing standard techniques. Two-dimensional quantitative coronary angiography analysis was performed using dedicated software package (CAAS 5.9; Pie Medical Imaging, Maastricht, Netherlands). The reference vessel diameter, minimal lumen diameter (MLD), percentage of diameter stenosis (%DS) and lesion length were measured by an experienced, independent investigator in a blind fashion.

Fractional Flow Reserve Measurement and Analysis.

The FFR measurements were done according to current guidelines.[18] A 0.014 inch pressure monitoring guidewire (Pressure Wire Certus, St. Jude Medical Uppsala, Sweden) was used for FFR measurement. All procedures were done after the administration of nitroglycerin. Maximal hyperemia was induced with a continuous intravenous infusion of adenosine (140 μg/kg/min).[19] The proximal and distal edge pressure from each lesion, which led to trans-stenotic step-up wave, were recorded during hyperemia. Vessel

FFR, proximal stenosis FFR and distal stenosis FFR were calculated at each point where pressure had been recorded, respectively. Trans-stenotic pressure gradient (△P) and FFR gradient (△FFR) were, then, calculated.

Intravascular Ultrasound Image's Acquisition and Analysis

IVUS images were obtained using commercially available systems (OptiCross^{TM}, Boston Scientific, USA or Volcano Therapeutics, Rancho Cordova, California, USA) after intracoronary administration of 200μg of nitroglycerine. The catheter was automatically pulled back at 0.5mm/s. IVUS images were analyzed using commercially available software (Echoplaque 4.0, INDEC Medical System, Santa Clara, California, USA) at a core laboratory (Seoul National University Hospital). Evaluation of lesion morphology and measurements of IVUS images were performed according to the American College of Cardiology Clinical Expert Consensus Document on Standard for Acquisition, Measurement and Reporting of Intravascular Ultrasound studies.[20,21] Quantitative IVUS parameters, lumen cross-sectional area (LA), external elastic

membrane area (EEMA), minimum lumen area (MLA), plaque plus media (P+M) area, have been measured. Plaque burden was calculated as [(EEMA – LA) / (EEMA)] x100. The remodeling index was calculated as: (EEMA at the MLA site) / (average of the proximal and distal reference EEMA), and positive remodeling was defined as a plaque with remodeling index ≥ 1.1. The reference site was the frame that showed the smallest plaque burden within 5 mm proximal and distal from the target lesions. The start and end points of the target lesions were defined as points of 50% plaque burden.[12]

Optical Coherence Tomography Image's Acquisition and Analysis

Optical coherence tomography pullbacks were obtained using commercially available OCT systems (Dragon Fly@, St. Jude Medical, USA). With a blood clearance by the injection of contrast medium, a 2.7F OCT imaging catheter was advanced distal to the lesion, and the entire length of region of interest was scanned using an integrated automated pullback device at 20mm/s. All OCT images were analyzed by 2 independent investigators (J.Z. and D.Y.H.). If

there was any discordance, a consensus reading was obtained. OCT images were analyzed with previously validated criteria for plaque characterization.[22] Fibrous plaque was defined as a signal-rich region with homogeneous scattering. Lipid plaque was defined as a diffusely bordered, signal-poor region with an overlying signal-rich band. Lipid-rich plaque was defined as the lipid arc subtended an angle $\geq 180^{\circ}$ in any of the cross-sectional images within each lesion. From lipid plaque, we measured lipid arc 3 times at its tentatively biggest angle frame, and the biggest value was considered. A lipid-rich plaque with a fibrous cap thickness $\leq$65 μm was defined as a thin cap fibroatheroma (TCFA).[23] Plaque rupture was defined as the presence of fibrous-cap discontinuity and a cavity formation in the plaque. Macrophage infiltration was defined as signal-intense punctuate regions with strong signal attenuation, and maximum arc of macrophage(s) was measured also 3 times to record the biggest one. Microvessel(s) were defined as signal-poor tubuloluminal structures including vasa vasorum, which were located in the adventitial layer, and intraplaque neovessels,

which were located in the plaque.[22,24,25]

Measurement of RG and APS

APS is a decomposing hemodynamic force from total hemodynamic force that based on the centerline direction of the vessel. Previous computational fluid dynamics (CFD) study proved that APS can be expressed as a function of pressure and RG. Such a RG can be used as not only a quantitative geometric descriptor but a surrogate marker of APS.[11] As the major gradient of pressure or FFR is most presented at upstream site but rarely at downstream site, we calculated the upstream APS by multiplying proximal pressure by the upstream RG and multiplying distal pressure by the distal RG for downstream one.[11,13]

RG, a geometric descriptor to quantitatively describe the axial changes in the legion geometry, was defined as dividing the radius change over lesion length. Radius change was the difference between radius of certain frame and MLA frame, and lesion length for calculating RG was the distance between those two frames.[11] For the RG calculation, we have performed several different

measurements. Firstly, *standard method*, the proximal and distal calculated points were defined as that of 2 mm inward from the edge of a target segments, has been used for measurement. And the start and end points of the target segment were defined as points of 50% plaque burden. Lesion length was measured from MLA to proximal (or distal) calculated point.[12] More methods have been used in our study. We predetermined the absolute calculated points (2.5 mm, 5 mm, 7.5 mm from MLA frame) to calculate RG in the same fashion. Reliability between RGs calculated utilizing standard method and those calculated on the absolute points was observed. "Upstream-dominant lesions" were defined as lesions with steeper radius change in upstream ($RG_{upstream} > RG_{downstream}$), whereas those with steeper radius change in downstream ($RG_{upstream} < RG_{downstream}$) were defined as "downstream-dominant lesions".[11,12] **(Fig. 2)**

Statistical Analysis

Continuous variables were expressed as median and interquartile range (IQR) and compared using Mann-Whitney U test, or mean ± standard deviation and compared using the Student t test.

Categorical variables were given as counts and percentages and compared using the chi-square test or Fisher exact test as appropriate. The intraclass correlation coefficient, Pearson's correlation analysis and Spearman's correlation analysis were used to assess the reliability and agreement between RGs calculated with standard measurement and RGs calculated with absolute distance - 2.5 mm, 5 mm and 7.5 mm, respectively. Cochran's Q test and McNemar test were used to compare the frequency of each vulnerable plaque features appearance as well as the frequency of maximum lipid arc appearance, maximum macrophage arc appearance and minimum cap thickness appearance among upstream segment, MLA segment and downstream segment in single lesion. All probability values were 2-sided and p-values < 0.05 were considered statistically significant. The statistical package SPSS, version 22.0 (SPSS Inc., Chicago, IL, USA) was used for statistical analyses.

Results

Baseline Characteristics of Patients

Thirty-eight patients with 38 lesions in OCT group and 33 patients with 35 lesions in IVUS group were enrolled (mean age 60.6 ± 10.1, male 77.5%, hypertension 49.3%, diabetes mellitus 35.2% hypercholesterolemia 54.9%, current smoker 23.9%, stable angina 39.4%, unstable angina 18.3%). The distribution of lesions was: left main to left anterior descending coronary artery (n = 60, 82.2%); left circumflex coronary artery (n = 5, 6.8%); right coronary artery (n = 8, 11.0%). The minimum lumen diameter, percent diameter stenosis, lesion length and reference vessel diameter were 1.34 ± 0.46, 49.77 ± 13.93%, 12.3 (8.49 - 15.77) and 2.62 ± 0.55, respectively (**Table 1**).

Reliability of RGs Calculated by Standard Measurement and Other Measurements

The intraclass correlation coefficient and correlation between RG measured utilizing standard method and RGs on 2.5 mm, 5 mm and 7.5 mm points were ICC = 0.859, r = 0.755 $p < 0.001$, ICC = 0.924 r = 0.904 $p < 0.001$ and ICC = 0.845 r = 0.878 $p < 0.001$, respectively (**Fig. 3**).

Hemodynamic Parameters in Lesions with or without Vulnerable Features

FFR, △FFR and △P according to lesions with or without vulnerable features are presented in Table 2. A significantly lower FFR was observed in the lesions with lipid rich plaque, detected by OCT, compared to those without lipid rich plaque [0.79(0.73-0.82) vs. 0.82(0.80-0.93) p = 0.038]. The △P was bigger in the lesions with microvessel(s), detected by OCT compared with those without microvessel(s) [12.5(8.0-21.3) vs. 7.5(5.0-14.8) p = 0.045]. The lesions with posterior attenuation, detected by IVUS, were showed bigger △FFR than those without posterior attenuation [0.19(0.11-

0.36) vs. 0.10(0.08-0.16) p = 0.038]. There were no significant differences regarding the other hemodynamic parameters according to other vulnerable features (**Table 2**).

Distribution of APSs in Upstream and Downstream Segments

For the total 73 lesions, 49 were upstream-dominant lesions, and the other 24 were downstream-dominant lesions. There were no significant differences in FFR, △P, △FFR, MLA and %DS between upstream-dominant lesions and downstream-dominant lesions [FFR: 0.82(0.73-0.88) vs. 0.80(0.75-0.84) p = 0.431; △P: 9.0(5.0-18.5) vs. 13.5(7.3-18.8) p = 0.160; △FFR: 0.11(0.07-0.175) vs. 0.15(0.07-0.19) p = 0.314; MLA: 2.34(1.83-3.22) vs. 2.24(1.69-2.75) p = 0.518; %DS: 50.5% ± 14.2% vs. 48.3% ± 13.5% p = 0.530, respectively]. However, APSs were significantly higher in the upstream segments of upstream-dominant lesions and downstream segments of downstream-dominant lesions than their counterparts. (upstream APS 9.78 ± 4.81 vs. 6.30 ± 3.89 p = 0.003; downstream APS 4.36 ± 2.68 vs. 8.25 ± 3.38 p < 0.001) (**Fig. 4. Table 3**).

Distribution of Vulnerable Features According to Longitudinal Lesion Asymmetry

In comparison of lipid rich plaque according to the longitudinal lesion asymmetry, the MLA segments showed a highest frequency among three segments within each lesion (upstream segments vs. MLA segments vs. downstream segments: 39.5% vs. 68.4% vs. 31.6% overall p = 0.001); a similar trend was observed in the upstream-dominant lesions (30.4% vs. 78.3% vs. 43.5% overall p = 0.002); whereas, downstream-dominant lesions showed a unique pattern (53.3% vs. 53.3% vs. 13.3% overall p = 0.011) (**Fig. 5A**) The composite of lipid rich plaque or posterior attenuated plaque showed a similar distribution compared to lipid rich plaque alone (all lesions: 24.7% vs. 47.9% vs. 24.7 overall p <0.001; upstream-dominant lesions: 18.4% vs. 46.9% vs. 30.6% overall p = 0.001; downstream-dominant lesions: 37.5% vs. 50.0% vs. 12.5% overall p = 0.005, respectively) (**Fig. 5B**). Conversely, no significant differences were shown among three segments with macrophage(s) (26.3% vs. 23.7% vs. 18.4 overall p = 0.646; 34.8% vs. 30.4% vs.

13.0% overall p = 0.148; 13.3% vs. 13.3% vs. 26.7% overall p = 0.449, respectively) (**Fig. 5C**) and with microvessel(s) (36.8% vs. 28.9% vs. 36.8% over p = 0.607; 30.4% vs. 30.4% vs. 34.8% overall p = 0.905; 46.7% vs. 26.7 vs. 40.0% overall p = 0.417, respectively) (**Fig. 5D**) (**Table 4**).

For the lipid plaque in total lesions, maximum lipid arc was most frequently observed in MLA segments, followed with upstream and downstream segments (upstream vs. MLA vs. downstream: 22.2% vs. 61.1% vs. 16.7% overall p = 0.002); upstream-dominant lesions presented another sequence (13.6% vs. 59.1% vs. 27.3% overall p = 0.028); for the downstream-dominant lesions, the downstream segments had few chances. (35.7% vs. 64.3% vs. 0% overall p = 0.013) (**Fig. 6A**). For the maximum lipid arc in addition to the maximum posterior attenuation arc, it was, also, showed a similar distribution (total lesions: 17.4% vs. 65.2% vs. 17.4% overall p < 0.001; upstream-dominant lesions: 10.7% vs. 60.7% vs. 28.6% overall p = 0.005; downstream-dominant lesions: 27.8% vs. 72.2% vs. 0% overall p = 0.001, respectively) (**Fig 6B**). But for the

macrophage, there was, though no statistical significance, a converse tendency compared to the lipid plaque (total lesions: 31.6% vs. 47.4% vs. 21.1% overall p = 0.036; upstream-dominant lesions: 41.7% vs. 58.3% vs. 0% overall p = 0.039; downstream-dominant lesions: 14.3% vs. 28.6% vs. 57.1% overall p = 0.368, respectively) (**Fig. 6C**). For the minimum cap thickness, another tendency was observed (total lesions: 36.1% vs. 50.0% vs. 13.9% p = 0.028; upstream-dominant lesions: 36.4% vs. 50.0% vs. 13.6% overall p = 0.108; downstream-dominant lesions: 35.7% vs. 50% vs. 14.3% overall p = 0.257, respectively) (**Fig. 6D**) (**Table 5**).

Discussion

The major finding of this study include: (1) hemodynamic parameters such as FFR, △FFR and △P showed differences between lesions with and without relevant vulnerable features; (2) standardly measured RGs can excellently be replaced by the RGs calculated on the points 5mm away from MLA; (3) each different vulnerable feature may have a different longitudinal distribution according to lesion asymmetry.

Role of Hemodynamic Force in Plaque Vulnerability

In our study, the coronary arteries with lower FFR had more chances that presence of lipid rich plaque. The FFR is an invasive

gold standard method to detect physiological significance of a coronary stenosis and can reduce the major adverse events in patients who undergoing percutaneous coronary intervention. However, whether it plays a role in presence of vulnerable plaque, which is a key part in the mechanism of rupture, is unclear. Only a little evidence was reported for such a significant issue, such as Chung et al.[26] and Brugaletta et al.[27] showed lower FFR vessels had more fibrofatty tissue in their virtual-histology intravascular ultrasound study; Shinchiro et al.[28], in their integrated backscatter intravascular ultrasound analysis, found that lipid plaque volume significantly negatively correlated with the FFR. These findings totally meet those of our study.

Furthermore, other two hemodynamic parameters, △FFR and △P per-lesion, were calculated in our study. We found that the lesions with microvessel(s), detected by OCT which has a superior resolution than IVUS, had smaller △P, and the lesions with posterior attenuation, detected by IVUS, presented bigger △FFR. Hemodynamic parameters, such as FFR, △FFR and △P, seem to

play a different role in detecting different plaque vulnerable features.

Availability of RG Calculated with Absolute Distance

The RG, an index of steepness in upstream or downstream segment, is basically calculated by the radius changes, between certain defined frame and MLA frame, divided by relevant length, between those two frames.[11,12] It firstly originated from computational fluid dynamics analysis of idealized model, and has been proven that highly correlated with APS.[11] Subsequently, another study was coming to explore the impact of longitudinal lesion geometry on location of rupture and clinical presentations using IVUS-measured RG. And lesion asymmetry assessed by RG was associated with the location of rupture and with clinical presentation.[12] Nevertheless, the current method of calculating RG was using the point of plaque burden 50% as the starting (or ending) point, so that OCT, which has the scarce information of EEM, should not able to measure RG utilizing the standard criteria. From current study, we could find that the RG calculated on point of

absolute distance away from MLA frame, especially 5mm, had a perfect reliability and a high correlation with standard one. Therefore, standard RG can totally be replaced by the RG_{5mm}. It largely supports the reasonability that measuring RG from OCT images, and combine with the OCT's outstanding ability of detecting plaque morphology, it should be more valuable in future study.

Distribution of APSs in Upstream and Downstream Segments.

Wall shear stress is a most well-known hemodynamic force, not only as it momentous role acting on the lesion initiation, progression and transformation but as the directly rupture-prone hemodynamic force. [6,9,14,15] Though WWS was mostly distributed on upstream or MLA site of lesion[13], Tanaka et al.[17] and Lee et al.[12] showed that not few ruptures were appeared on downstream plaque in their IVUS study. However, magnitude of APS can be extremely greater, even several decade times, than that of WSS, in addition, such a magnitude in the downstream segment seems to be as great as upstream segment unlike WSS, pressure and FFR.[11] Such a

situation may interpret the reason of downstream rupture ' s occurrence.[12] According to the APS derivation reported in previous study[11], APS was first time calculated using invasively measured data in our study. Upstream APS is multiplying upstream RG by proximal pressure and downstream APS is multiplying downstream RG by downstream pressure. Even though there were no difference between upstream-dominant and downstream-dominant lesions in their FFR, △FFR, △P, MLA and %DS, the APS was significantly higher in the upstream segments of upstream-dominant lesions and downstream segment of downstream-dominant lesions than their counterparts. It became possible that lively calculating the APS when PCI is ongoing. These hemodynamic as well as geometric indices may be helpful to make a more reasonable clinical decision.

Longitudinal Distribution of Vulnerable Plaque Features

Recent studies provided many reasonable scenarios to explain the key role of WSS for plaque vulnerability and rupture. With the context of WSS, we hypothesized that APS, which appears greater magnitude of force, might be another potential and

significant factor of plaque's progression, distribution and transformation. The APSs correlated highly with RGs, whereas several different distributional tendencies were observed depending upon different vulnerable features. To compare presence of vulnerable features in upstream and downstream segments, as well as to avoid the homogeneous features in boundary of adjacent segment, a longitudinal tertile comparison was performed in a single lesion. Each lesion was divided into three segment – upstream segment, MLA segment and downstream segment. MLA segment was the 5mm-long segment within center of MLA slide. And the other two segments were the outward of MLA segment in every single lesion. Lipid rich plaque, of course, most frequently presented in MLA segment. However, the presence of vulnerable plaque was negatively associated with its RG-domination, that is, the higher RG segment showed a lower frequency of vulnerable plaque. Equally, in addition to posterior attenuated plaque detected by IVUS, a consistent situation like lipid rich plaque alone was observed. The presence of macrophage was positively associated

with lesion asymmetry not with presence of microvessel(s).

OCT-detected maximum lipid arc alone with or without IVUS-detected maximum posterior attenuation arc or maximum macrophage arc appeared similar tendency, when examining the vulnerable features of the plaque. Minimum cap thickness was consistently observed in upstream segment regardless of plaque asymmetry.

APS and RG seem not to play a crucial role in distribution of vulnerable features as we hypothesized, which means the force of APS directly impacting on plaque might contribute to plaque rupture only

Conclusion

Hemodynamic parameters, FFR, △FFR and △P show differences between lesions with and without lipid rich plaque, microvessel(s) and posterior attenuation. While, APS seems not to play a crucial role in distribution of vulnerable features, its force directly impacting on plaque appears to contribute to plaque rupture only.

References

1. Dirksen MT, van der Wal AC, van den Berg FM, et al. Distribution of inflammatory cells in atherosclerotic plaques relates to the direction of flow. Circulation 1998;98:2000-3.

2. Kolodgie FD, Virmani R, Burke AP, et al. Pathologic assessment of the vulnerable human coronary plaque. Heart (British Cardiac Society) 2004;90:1385-91.

3. Hong MK, Mintz GS, Lee CW, et al. The site of plaque rupture in native coronary arteries: a three-vessel intravascular ultrasound analysis. Journal of the American College of Cardiology 2005;46:261-5.

4. Rodriguez-Granillo GA, Garcia-Garcia HM, Valgimigli M, et al. Global characterization of coronary plaque rupture phenotype using three-vessel intravascular ultrasound radiofrequency data analysis. European heart journal 2006;27:1921-7.

5. Cheruvu PK, Finn AV, Gardner C, et al. Frequency and distribution of thin-cap fibroatheroma and ruptured plaques in human coronary arteries: a pathologic study. Journal of the American College of Cardiology 2007;50:940-9.

6. Fukumoto Y, Hiro T, Fujii T, et al. Localized elevation of shear stress is related to coronary plaque rupture: a 3-dimensional intravascular ultrasound study with in-vivo color mapping of shear stress distribution. Journal of the American College of Cardiology 2008;51:645-50.

7. Hong MK, Mintz GS, Lee CW, et al. A three-vessel virtual histology intravascular ultrasound analysis of frequency and distribution of thin-cap fibroatheromas in patients with acute coronary syndrome or stable angina pectoris. The American journal of cardiology 2008;101:568-72.

8. Cicha I, Worner A, Urschel K, et al. Carotid plaque vulnerability: a positive feedback between hemodynamic and biochemical mechanisms. Stroke 2011;42:3502-10.

9. Li ZY, Howarth SP, Tang T, Gillard JH. How critical is fibrous cap thickness to carotid plaque stability? A flow-plaque interaction model. Stroke 2006;37:1195-9.

10. Li ZY, Gillard JH. Plaque rupture: plaque stress, shear stress, and pressure drop. Journal of the American College of Cardiology 2008;52:1106-7; author reply 7.

11. Choi G, Lee JM, Kim HJ, et al. Coronary Artery Axial Plaque Stress and its Relationship With Lesion Geometry: Application of Computational Fluid Dynamics to Coronary CT Angiography. JACC Cardiovascular imaging 2015;8:1156-66.

12. Lee JM, Choi G, Hwang D, et al. Impact of Longitudinal Lesion Geometry on Location of Plaque Rupture and Clinical Presentations. JACC Cardiovascular imaging 2016.

13. Park JB, Choi G, Chun EJ, et al. Computational fluid dynamic

measures of wall shear stress are related to coronary lesion characteristics. Heart (British Cardiac Society) 2016;102:1655-61.

14. Samady H, Eshtehardi P, McDaniel MC, et al. Coronary artery wall shear stress is associated with progression and transformation of atherosclerotic plaque and arterial remodeling in patients with coronary artery disease. Circulation 2011;124:779-88.

15. Dolan JM, Kolega J, Meng H. High wall shear stress and spatial gradients in vascular pathology: a review. Annals of biomedical engineering 2013;41:1411-27.

16. Doriot PA. Estimation of the supplementary axial wall stress generated at peak flow by an arterial stenosis. Physics in medicine and biology 2003;48:127-38.

17. Tanaka A, Shimada K, Namba M, et al. Relationship between longitudinal morphology of ruptured plaques and TIMI flow grade in acute coronary syndrome: a three-dimensional intravascular ultrasound imaging study. European heart journal 2008;29:38-44.

18. Pijls NH, De Bruyne B, Peels K, et al. Measurement of fractional flow reserve to assess the functional severity of coronary-artery stenoses. The New England journal of medicine 1996;334:1703-8.

19. Jang HJ, Koo BK, Lee HS, et al. Safety and efficacy of a novel hyperaemic agent, intracoronary nicorandil, for invasive physiological assessments in the cardiac catheterization laboratory. European heart journal 2013;34:2055-62.

20. Mintz GS, Nissen SE, Anderson WD, et al. American College of Cardiology Clinical Expert Consensus Document on Standards for Acquisition, Measurement and Reporting of Intravascular Ultrasound Studies (IVUS). A report of the American College of Cardiology Task Force on Clinical Expert Consensus Documents. Journal of the American College of Cardiology 2001;37:1478-92.

21. Maehara A, Mintz GS, Bui AB, et al. Morphologic and angiographic features of coronary plaque rupture detected by intravascular ultrasound. Journal of the American College of Cardiology 2002;40:904-10.

22. Tearney GJ, Regar E, Akasaka T, et al. Consensus standards for acquisition, measurement, and reporting of intravascular optical coherence tomography studies: a report from the International Working Group for Intravascular Optical Coherence Tomography Standardization and Validation. Journal of the American College of Cardiology 2012;59:1058-72.

23. Yabushita H, Bouma BE, Houser SL, et al. Characterization of human atherosclerosis by optical coherence tomography. Circulation 2002;106:1640-5.

24. Kato K, Yonetsu T, Kim SJ, et al. Comparison of nonculprit coronary plaque characteristics between patients with and without diabetes: a 3-vessel optical coherence tomography study. JACC Cardiovascular interventions 2012;5:1150-8.

25. Taruya A, Tanaka A, Nishiguchi T, et al. Vasa Vasorum Restructuring in Human Atherosclerotic Plaque Vulnerability: A Clinical Optical Coherence Tomography Study. Journal of the American College of Cardiology 2015;65:2469-77.

26. Chung JH, Ann SH, Singh GB, et al. Segmental assessments of coronary plaque morphology and composition by virtual histology intravascular ultrasound and fractional flow reserve. The international journal of cardiovascular imaging 2016;32:373-80.

27. Brugaletta S, Garcia-Garcia HM, Shen ZJ, et al. Morphology of coronary artery lesions assessed by virtual histology intravascular ultrasound tissue characterization and fractional flow reserve. The international journal of cardiovascular imaging 2012;28:221-8.

28. Sakurai S, Takashima H, Waseda K, et al. Influence of plaque characteristics on fractional flow reserve for coronary lesions with

intermediate to obstructive stenosis: insights from integrated-backscatter intravascular ultrasound analysis. The international journal of cardiovascular imaging 2015;31:1295-301.

Figure 1 Study Flow

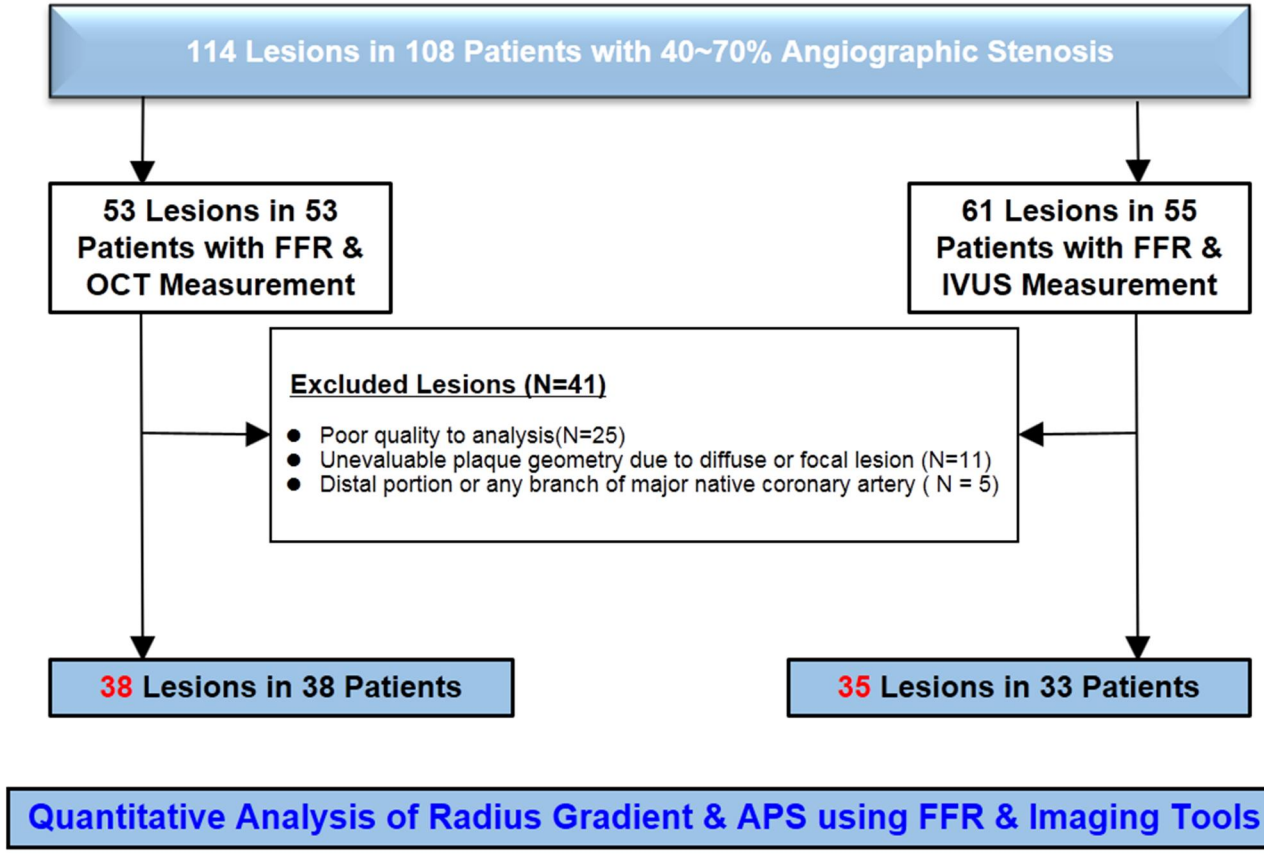

Study flow and reasons for exclusion are presented. The 73 lesions are classified as upstream-dominant lesion or downstream-dominant lesion according to lesion asymmetry. FFR = fractional flow reserve, OCT = optical coherence tomography, IVUS = intravascular ultrasound, APS = axial plaque stress.

Figure 2 Example of IVUS Measurements and Standard RG Derivation

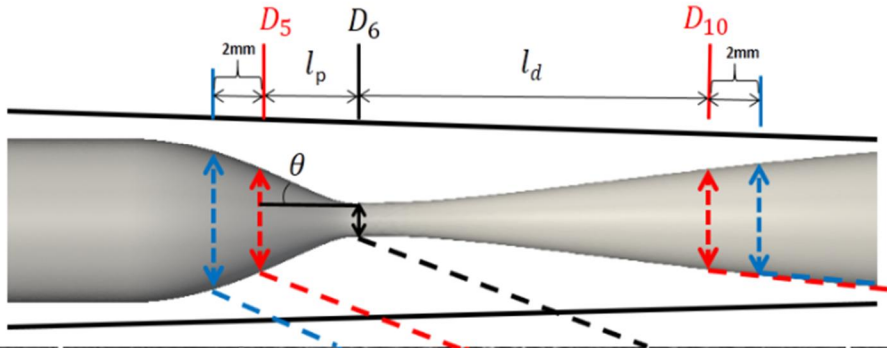

$$RG_{upstream} = \frac{D_5 - D_6}{l_p}$$

$$RG_{downstream} = \frac{D_6 - D_{10}}{l_d}$$

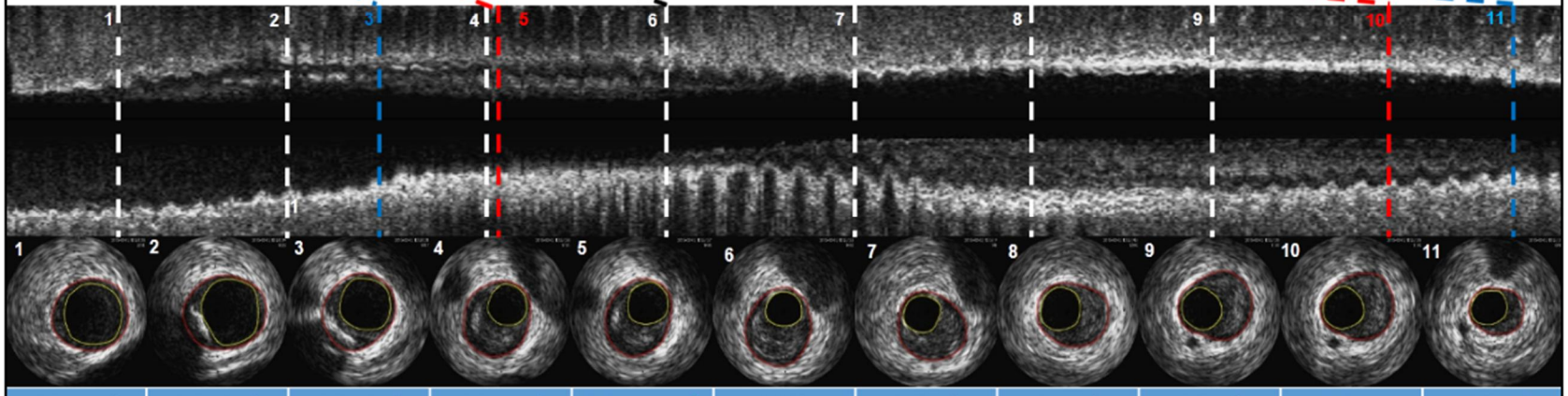

1. Proximal 7.5mm	2. Proximal 5mm	3. Proximal 50%PB	4. Proximal 2.5mm	5. 2mm Inward from [3]	6. MLA	7. Distal 2.5mm	8. Distal 5mm	9. Distal 7.5mm	10. 2mm Inward from [11]	11. Distal 50%PB
LA 13.04mm^2	LA 13.76mm^2	LA 9.66mm^2	LA 5.79mm^2	LA 5.94mm^2	LA 4.54mm^2	LA 4.71mm^2	LA 6.25mm^2	LA 5.9mm^2	LA 6.04mm^2	LA 4.55mm^2
EEM 20.19mm^2	EEM 21.32mm^2	EEM 19.65mm^2	EEM 18.60mm^2	EEM 18.24mm^2	EEM 18.39mm^2	EEM 16.3mm^2	EEM 16.73mm^2	EEM 18.07mm^2	EEM 17.39mm^2	EEM 9.41mm^2
PB 35.4%	PB 35.4%	PB 50.8%	PB 68.8%	PB 67.4%	PB 75.3%	PB 71.1%	PB 62.6%	PB 67.3%	PB 65.3%	PB 51.7%

Standard measurement: the RGs in which points of 2mm inward of 50% plaque burden frame were calculated. Other measurements: The RGs in which 2.5mm, 5mm, 7.5mm away from MLA were calculated respectively. IVUS = intravascular ultrasound, RG = radius gradient, MLA = minimal lumen area, LA = lumen area, EEM = external elastic membrane, PB = plaque burden.

Figure 3 **Reliability of RGs Calculated by Standard Measurement and Other Measurement**

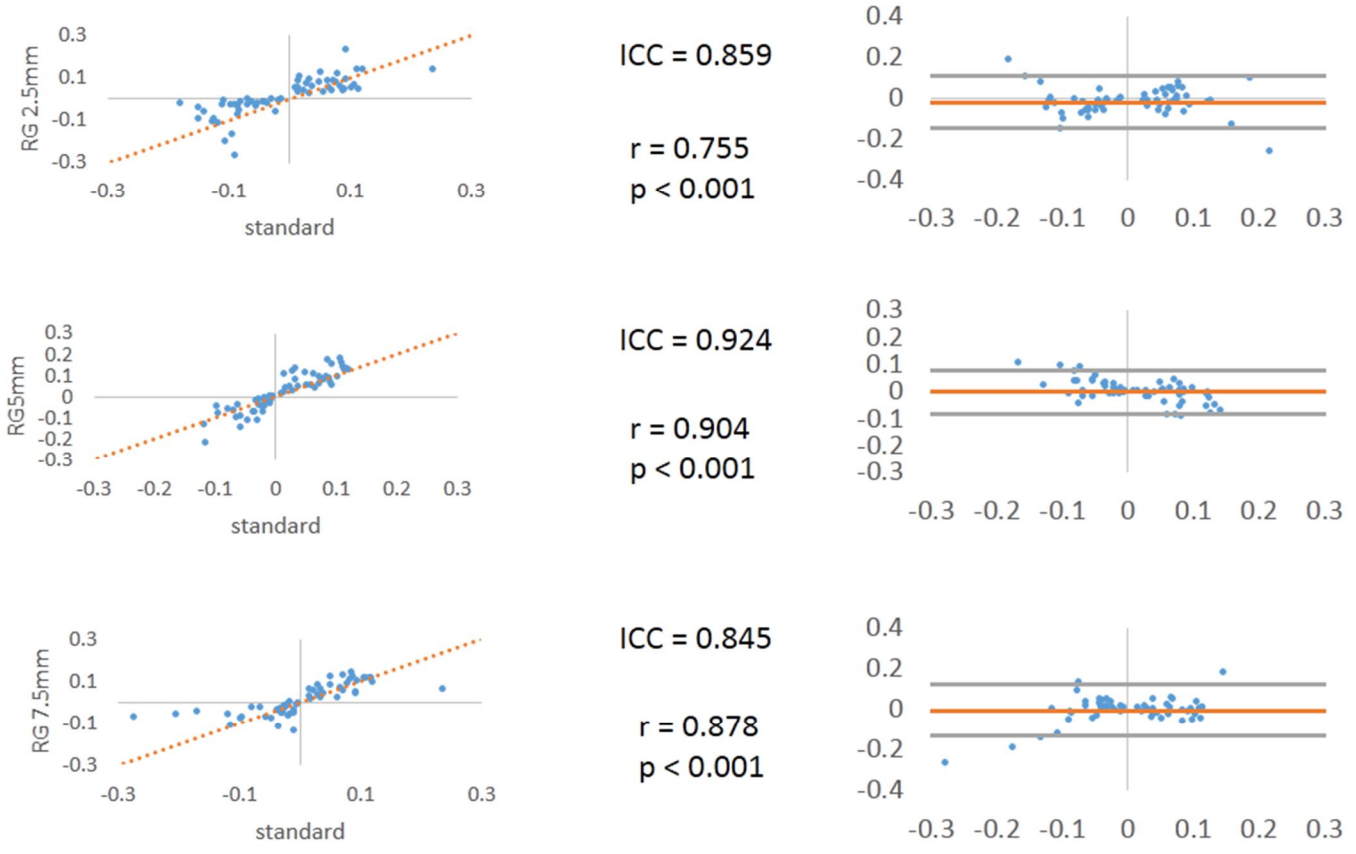

Excellent intraclass correlation coefficient is observed in each point we predetermined, and the RG on 5 mm point is the best. RG = radius gradient, ICC = intraclass correlation coefficient.

Figure 4 Distribution of RG and APS According to Lesion Asymmetry

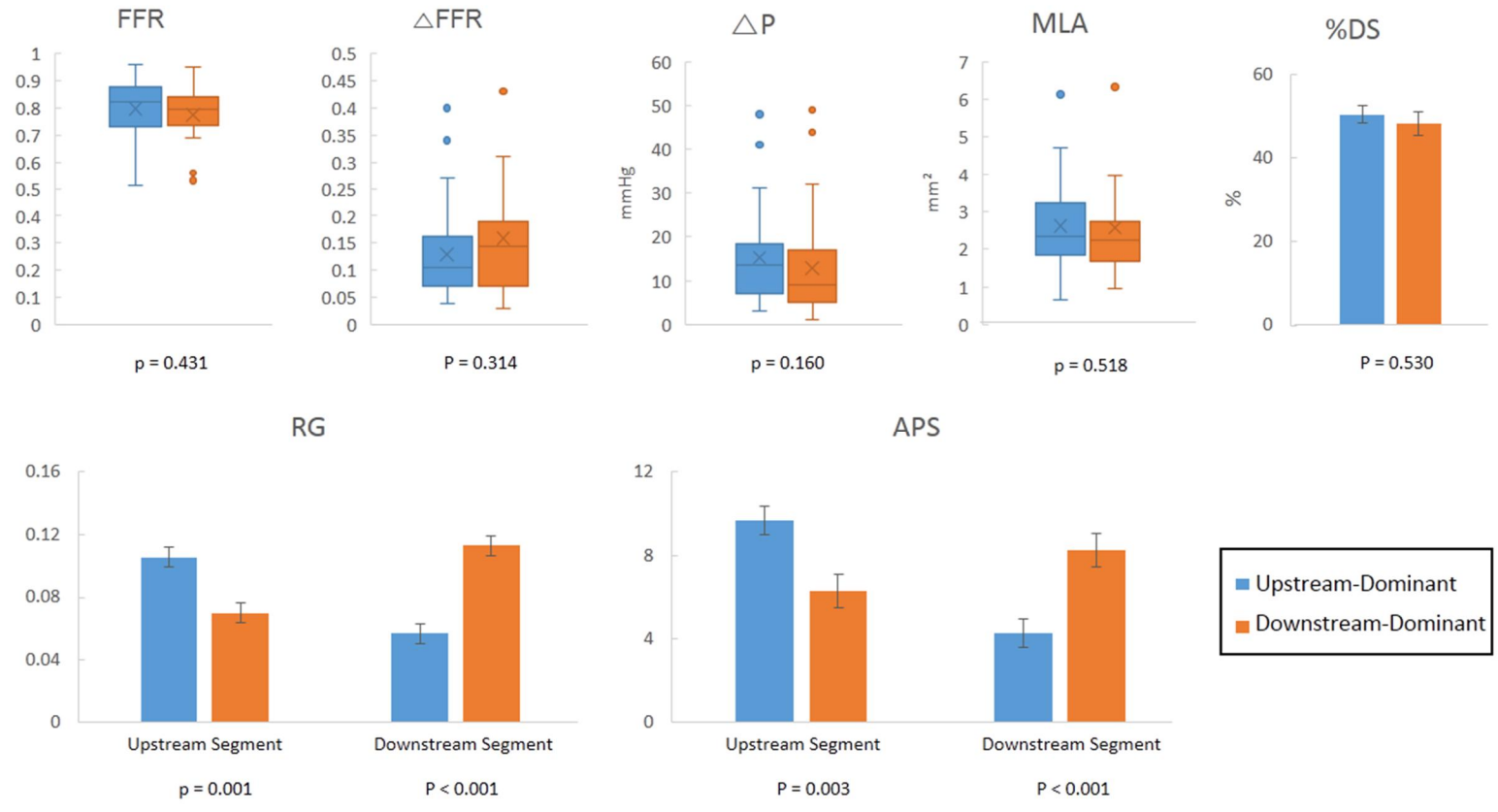

Although FFR, △FFR, △P, MLA, %DS are no significant differences between upstream-dominant and downstream dominant lesions, higher APS are distributed in upstream segments of upstream-dominant lesions and downstream segments of downstream-dominant lesions. RG = radius gradient, APS = axial plaque stress, FFR = fractional flow reserve, △FFR = trans-stenotic FFR gradient, △P = trans-stenotic pressure gradient, MLA = minimal lumen area, %DS = percentage of diameter stenosis.

Figure 5 Distribution of Vulnerable Features According to Longitudinal Lesion Asymmetry

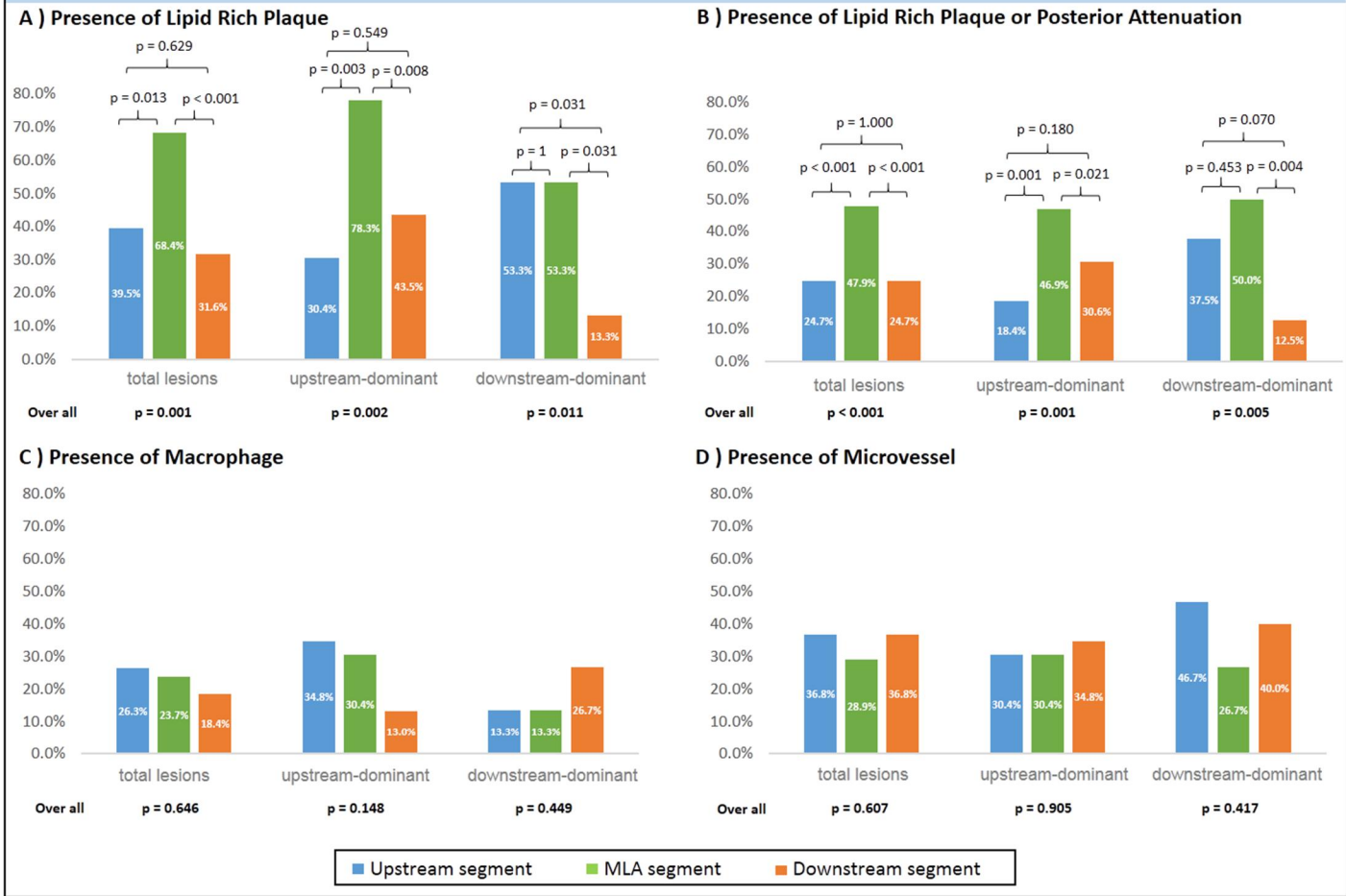

Most lipid rich plaque and posterior attenuated plaque are presented in MLA segments. There is a tendency that upstream-dominant lesions have less lipid rich plaque in their upstream segments than downstream segments, but downstream-dominant lesions have less lipid rich plaque in their downstream segments than upstream segments. Macrophage is more frequently observed in the upstream segments of upstream-dominant lesions and downstream segments of downstream-dominant lesions. Nevertheless there seems to be no differences in presence of microvessel. MLA = minimal lumen area.

Figure 6 Distribution of Vulnerable Features According to Longitudinal Lesion Asymmetry

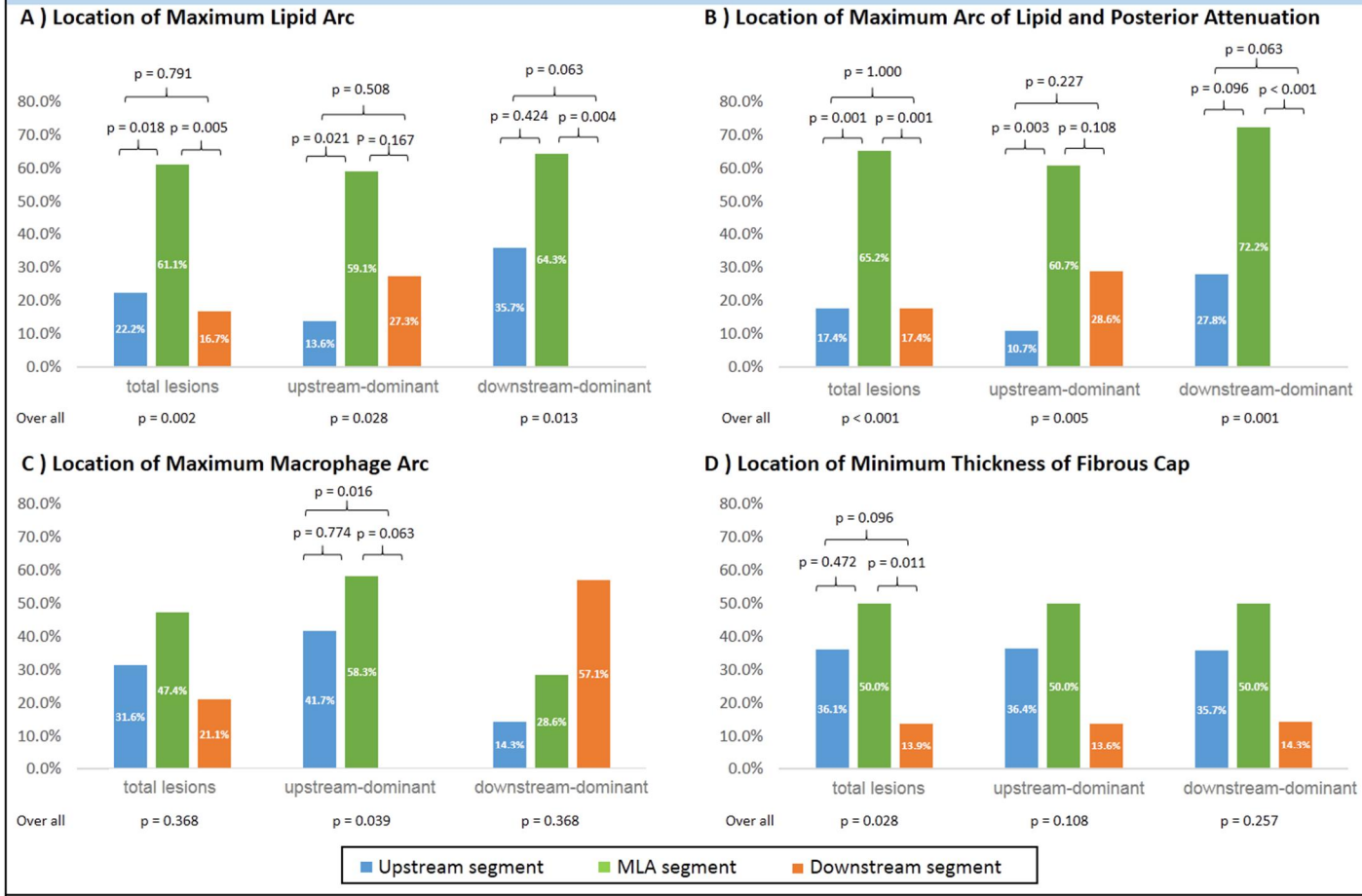

Maximum lipid arc and posterior attenuation arc are most frequently observed in the MLA segments. Interestingly, there is a tendency that upstream dominant lesions have less chances of presenting maximum lipid arc in their upstream segments than downstream, and downstream-dominant lesions have less chance in their downstream segments than upstream segments. However, for the macrophage, maximum arc is more frequently detected in upstream segments of upstream-dominant lesions and downstream segments of downstream-dominant lesions. For the cap thickness, there consistently is more chances that upstream segments have the thinnest cap regardless of lesion asymmetry. OCT = optical coherence tomography, MLA = minimal lumen area.

Table 1 Patient and Lesion Characteristics	
Patients (n = 71)	
Age, years	60.6 ± 10.1
Male	55 (77.5%)
Cardiovascular Risk Factors	
Hypertension	35 (49.3%)
Diabetes mellitus	25 (35.2%)
Hypercholesterolemia	39 (54.9%)
Current smoker	17 (23.9%)
Clinical Presentations	
Stable angina	28 (39.4%)
Unstable angina	13 (18.3%)
Others	30 (42.3%)
Lesion characteristics (n = 73)	
Lesion locations	
Left main to LAD	60(82.2%)
LCX	5 (6.8%)
RCA	8 (11.0%)
Quantitative coronary angiography	
Reference vessel diameter (mm)	2.62 ± 0.55
Minimal lumen diameter (mm)	1.34 ± 0.46
Diameter stenosis (%)	49.77 ± 13.93
Lesion length (mm)	12.30 (8.49–15.77)

Values are mean ± SD or n(%)
LAD = left anterior descending artery; LCX = left circumflex artery; RCA = right coronary artery

Table 2 Comparison of FFR, △FFR, △P According to OCT- or IVUS-defined Plaque Characteristics

	FFR			△FFR			△P		
	Absence	Presence	p Value	Absence	Presence	p Value	Absence	Presence	p Value
OCT-defined plaque characteristics (lesion n=38)									
TCFA	0.80(0.74-0.84)	0.79(0.74-0.86)	0.900	0.12(0.06-0.20)	0.07(0.06-0.09)	0.069	11.0(7.0-20.5)	8.0(4.5-10.0)	0.159
Macrophage	0.79 ± 0.09	0.80 ± 0.08	0.706	0.13 ± 0.08	0.12 ± 0.06	0.464	13.9 ± 8.9	11.9 ± 8.1	0.485
Prominent microvessels	0.80(0.71-0.84)	0.80(0.74-0.83)	0.693	0.09(0.06-0.14)	0.12(0.07-0.20)	0.181	7.5(5.0-14.8)	12.5(8.0-21.3)	0.045
Lipid rich plaque	0.82(0.80-0.93)	0.79(0.73-0.82)	0.038	0.09(0.06-0.14)	0.12(0.06-0.20)	0.343	8.0(6.0-12.5)	12.5(7.0-21.0)	0.142
IVUS-defined plaque characteristics (lesion n=35)									
Posterior attenuation	0.83(0.74-0.86)	0.78(0.57-0.85)	0.240	0.10(0.08-0.16)	0.19(0.11-0.36)	0.038	10.0(5.0-15.5)	13.5(5.8-45.0)	0.358
Positive remodeling	0.81(0.72-0.85)	0.87(0.65-0.91)	0.356	0.12(0.09-0.21)	0.12(0.08-0.18)	0.782	10.0(5.5-23.0)	11.0(1.5-19.0)	0.564

Values are mean ± SD or n(%)

FFR = fractional flow reserve; △FFR = trans-stenotic FFR gradient; △P = trans-stenotic pressure gradient; IVUS = intravascular ultrasound; MLA = minimal lumen area; OCT = optical coherence tomography; TCFA = thin-cap fibroatheroma

Table 3 Distribution of RG and APS According to Lesion Asymmetry

	Upstream-dominant Lesions	Downstream-dominant lesions	p Value
FFR	0.82(0.73-0.88)	0.80(0.75-0.84)	0.431
△FFR	0.11(0.07-0.18)	0.15(0.07-0.19)	0.314
△P (mmHg)	9.0(5.0-18.5)	13.5(7.3-18.8)	0.160
MLA (mm^2)	2.34(1.83-3.22)	2.24(1.69-2.75)	0.518
%DS (%)	50.5 ± 14.2	48.3 ± 13.5	0.530

	Upstream segment			Downstream segment		
	Upstream-dominant Lesions	Downstream-dominant Lesions	p Value	Upstream-dominant Lesions	Downstream-dominant Lesions	p Value
RG	0.106 ± 0.045	0.070 ± 0.040	0.001	0.058 ± 0.036	0.113 ± 0.044	<0.001
APS (mmHg)	9.78 ± 4.81	6.30 ± 3.89	0.003	4.36 ± 2.68	8.25 ± 3.38	<0.001

Values are mean ± SD or median (interquartile range)
FFR = fractional flow reserve; △FFR = trans-stenotic FFR gradient; △P = trans-stenotic pressure gradient; IVUS = intravascular ultrasound; MLA = minimal lumen area; %DS = percent diameter stenosis; RG = radius gradient; APS = axial plaque stress

Table 4 Distribution of Vulnerable Features According to Longitudinal Lesion Asymmetry

	Upstream Segment	MLA Segment	Downstream Segment	Overall p Value	Upstream vs. MLA p Value	MLA vs. Downstream p Value	Upstream vs. Downstream p Value
Presence of Lipid Rich Plaque (%)							
Total lesions (n = 38)	15(39.5)	26(68.4)	12(31.6)	0.001	0.013	<0.001	0.692
Upstream-dominant lesions (n = 23)	7(30.4)	18(78.3)	10(43.5)	0.002	0.003	0.008	0.549
Downstream-dominant lesions (n = 15)	8(53.3)	8(53.3)	20(13.3)	0.011	1	0.031	0.031
Presence of Lipid Rich Plaque or Posterior Attenuation (%)							
Total lesions (n = 73)	18(24.7)	35(47.9)	18(24.70	<0.001	<0.001	<0.001	1
Upstream-dominant lesions (n = 49)	9(18.4)	23(46.9)	15(30.6)	0.001	0.001	0.021	0.180
Downstream-dominant lesions (n = 24)	9(37.5)	12(50.0)	3(12.5)	0.005	0.453	0.004	0.070
Presence of Macrophage(s) (%)							
Total lesions (n = 38)	10(26.3)	9(23.7)	7(18.4)	0.646			
Upstream-dominant lesions (n = 23)	8(34.8)	7(30.4)	3(13.0)	0.148			
Downstream-dominant lesions (n = 15)	2(13.3)	2(13.3)	4(23.7)	0.449			
Presence of Microvessel(s) (%)							
Total lesions (n = 38)	14(36.8)	11(28.9)	14(36.8)	0.607			
Upstream-dominant lesions (n = 23)	7(30.4)	7(30.4)	8(34.8)	0.905			
Downstream-dominant lesions (n = 15)	7(46.7)	4(26.7)	6(40.4)	0.417			

Values are counts (percentages)
MLA = minimal lumen area.

Table 5 Distribution of Vulnerable Features According to Longitudinal Lesion Asymmetry

	Upstream Segment	MLA Segment	Downstream Segment	Overall p Value	Upstream vs. MLA p Value	MLA vs. Downstream p Value	Upstream vs. Downstream p Value
Frequency of Appearance of Maximum Lipid Arc							
Total lesions (n = 36)	8(22.2)	22(61.1)	6(16.7)	0.002	0.018	0.005	0.791
Upstream-dominant lesions (n = 22)	3(13.6)	13(59.1)	6(27.3)	0.028	0.021	0.167	0.508
Downstream-dominant lesions (n = 14)	5(35.7)	9(64.3)	0	0.013	0.424	0.004	0.063
Frequency of Appearance of Maximum Lipid Arc or Maximum Posterior Attenuation Arc							
Total lesions (n = 46)	8(17.4)	30(65.2)	6(17.4)	<0.001	0.001	0.001	1
Upstream-dominant lesions (n = 28)	3(10.7)	17(60.7)	8(28.6)	0.005	0.003	0.108	0.227
Downstream-dominant lesions (n = 18)	5(27.8)	13(72.2)	0	0.001	0.096	<0.001	0.063
Frequency of Appearance of Maximum Macrophage(s) Arc							
Total lesions (n = 19)	6(31.6)	9(47.4)	4(21.1)	0.368			
Upstream-dominant lesions (n = 12)	5(41.7)	7(58.3)	0	0.039	0.774	0.063	0.016
Downstream-dominant lesions (n = 7)	1(14.3)	2(28.6)	4(57.1)	0.368			
Frequency of Appearance of Thinnest Fibrous Cap							
Total lesions (n = 36)	13(36.1)	18(50.0)	5(13.9)	0.028	0.472	0.011	0.096
Upstream-dominant lesions (n = 22)	8(36.4)	11(50.0)	3(13.6)	0.108			
Downstream-dominant lesions (n = 14)	5(35.7)	7(50.0)	2(14.3)	0.257			

Values are counts (percentages)
MLA = minimal lumen area.

국문초록

목적: 관상동맥 협착 병변의 형태 및 혈류역학적 지표가 동맥경화반의 취약성에 미치는 영향을 관찰하고자 연구를 진행하였다.

배경: 동맥경화반 자체의 형태학적, 조직학적 특징과 동맥경화반의 취약성의 관련성에 대한 연구는 많았으나 관상동맥 협착 병변의 형태 및 혈류역학적 지표가 동맥경화반의 취약성에 미치는 영향에 대해선 잘 알려져 있지 않다.

방법 및 결과: 관상동맥조영술에서 40~70%협착을 보이는 환자 중 동시에 분획혈류예비량 및 침습적 영상검사 [Optical coherence tomography(OCT) or Intravascular ultrasound(IVUS)] 를 시행한 71명의 환자(73개 병변)에서 관찰연구를 진행하였다. 혈관의 분획혈류예비량 [fractional flow reserve(FFR)] 은 lipid rich plaque이 있는 혈관에서 없는 혈관보다 현저히 낮았고 [0.79(0.73-0.82) vs. 0.82(0.80-0.93) p=0.038]; 압력의 변화 (△P) 는 microvessel(s)이 있는 병변에서 컸고 [12.5(8.0-21.3) vs. 7.5(5.0-14.8) p=0.045]; 분획혈류예비량의 변화 (△FFR) 는 조영감쇄 죽상경화반(posterior attenuation)이 있는 병변에서 컸다 [0.19(0.11-0.36) vs. 0.10(0.08-0.16)]. Minimum lumen area(MLA) 와 5mm 떨어진 곳에서 측정한 Radius gradient(RG)는 선행 연구에서 계산한 방법으로 계산한 RG와 높은 재현성과 상관성을 보였다 [intraclass correlation coefficient (ICC) = 0.924; r = 0904 p < 0.001]. Downstream-dominant 병변에서 lipid rich plaque 및 조영감쇄는 downstream segment에서 제일 적게 관찰되었고 (upstream vs.

MLA vs. downstream 53.3% vs. 53.3% vs. 13.3% p = 0.011); maximum lipid arc 역시 downstream에서 제일 적게 관찰되었다 (upstream vs. MLA vs. downstream 35.7% vs. 64.3% vs. 0% p = 0.013).

결론: 혈류역학적 지표인 분획혈류예비력, 분획혈류예비력의 변화, 압력의 변화는 각각 lipid rich plaque, microvessel(s), 조영감쇄의 유무에 따라서 차이를 보였다. 종축 전단력 [axial plaque stress(APS)]은 관상동맥 병변 취약성의 분포에 영향을 주지 않았다.

주요어: 관상동맥 죽상경화반; 죽상경화반 취약성; 분획혈류예비력; Radius gradient; 종축 전단력; 혈관내 초음파; 광간섭 단층촬영.

학번: 2015-22406